Supplementary Information

Label-free metabolic imaging for sensitive and robust monitoring of anti-CD47 immunotherapy response in triple-negative breast cancer

Minfeng Yang[1], Arpan Mahanty[1], Chunjing Jin[2], Alex Ngai Nick Wong[1], Jung Sun Yoo[1]*

[1]Department of Health Technology and Informatics, The Hong Kong Polytechnic University, Kowloon, Hong Kong

[2]Laboratory Medicine Center, The Affiliated Chuzhou Hospital of Anhui Medical University, The First People's Hospital of Chuzhou, Chuzhou, China.

***Correspondence to** Dr Jung Sun Yoo; jungsun.yoo@polyu.edu.hk, Tel: +852-3400-8654, Address: Room Y905, 9/F, Lee Shau Kee Building, The Hong Kong Polytechnic University, Hung Hom, Kowloon, Hong Kong

List of Supplementary Items

Supplementary Figure 1

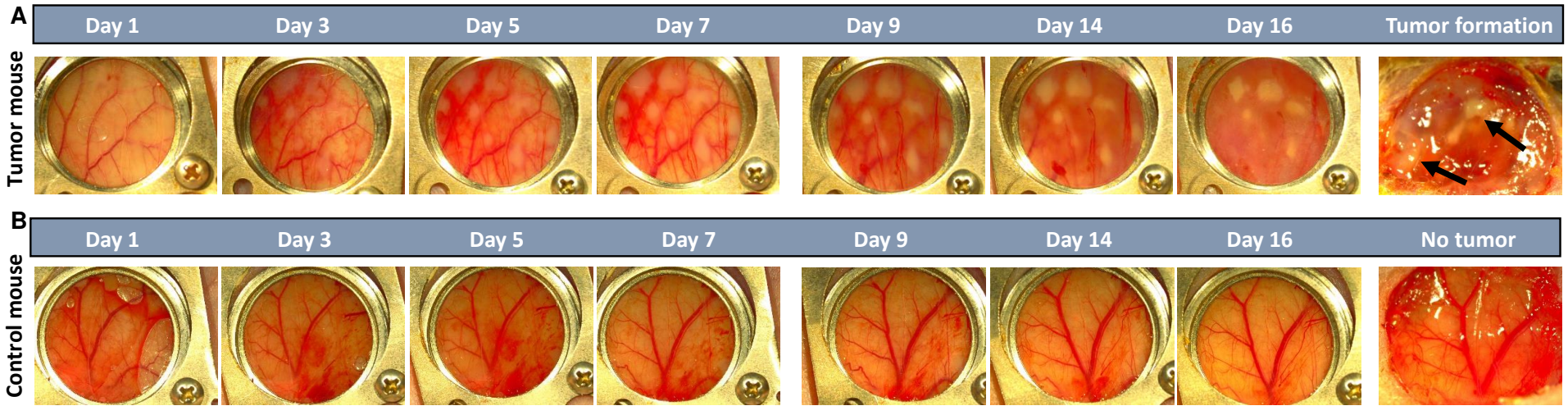

Development of a murine skinfold model of triple-negative breast cancer. A whole course of time-lapse anatomical imaging of tumor growth in a mouse skinfold window chamber model of triple-negative breast cancer **(A)** by comparison with a control mouse **(B)**. Color anatomy shows formation of tumor nodules and angiogenesis in a skinfold window chamber of a tumor model in a course of 16 days compared to a control mouse. Tumor formation was clearly confirmed after removing the window chamber (arrows).

Supplementary Figure 2

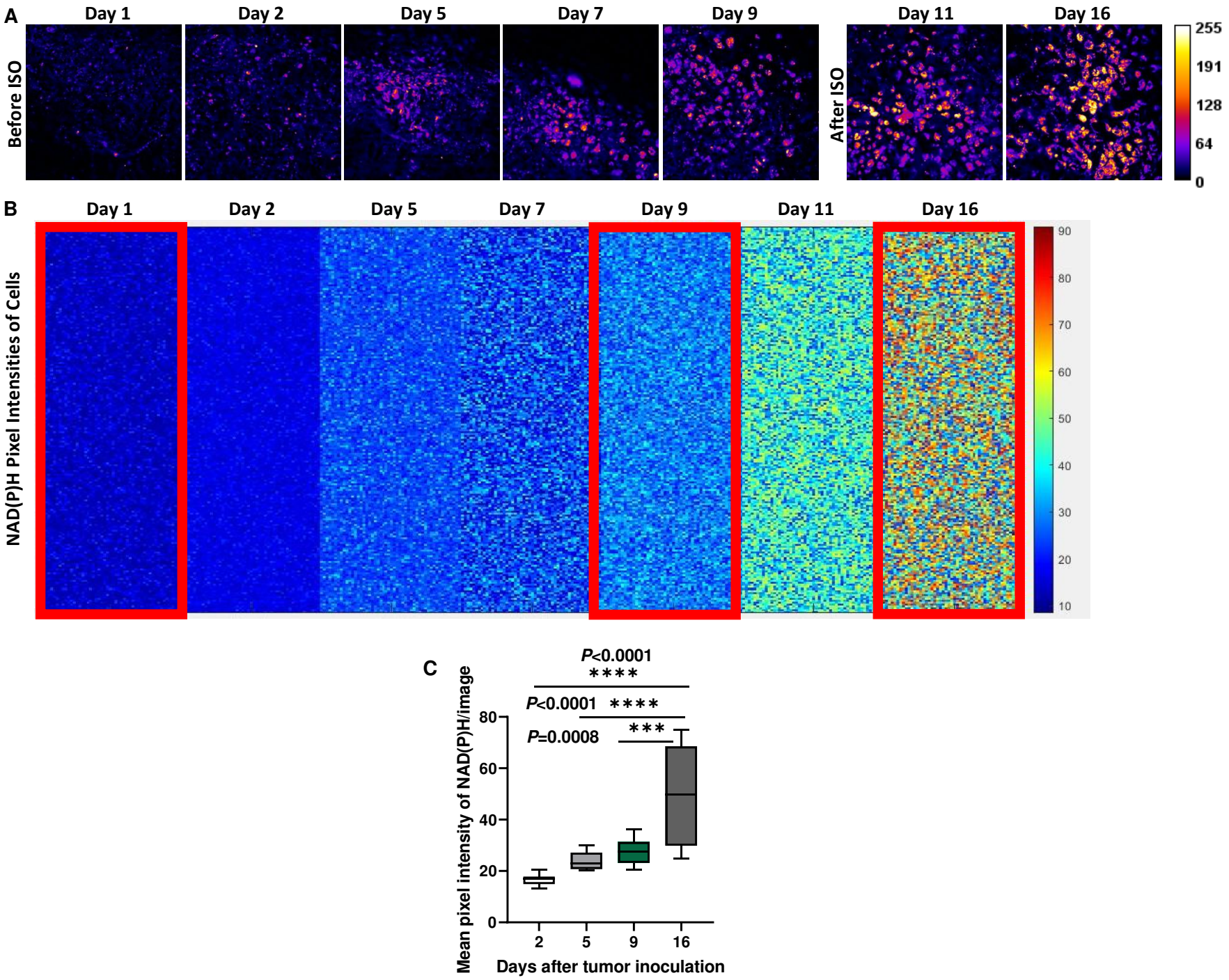

Dynamic metabolic imaging of NAD(P)H before and after treatment of isotype control antibody. **(A)** Label-free metabolic intravital imaging (LMMI) of NAD(P)H before and after treatment of isotype control antibody showing continuous tumor growth (10 mg/kg intravenous injection daily for 5 days). **(B)** Kinetics of single cell metabolism with NAD(P)H signal. Each colored small square represents the visible pixel intensity of NAD(P)H in each cancer cell. 10,000-pixel intensities were randomly measured from the cells in different mice every day for 16 days (n=5 mice). Metabolic signal of NAD(P)H has been increased with tumor growth from Day 1 to Day 9 and continued to increase even with start of isotype control treatment from Day 10 as expected. **(C)** Quantification of average intensity shows clear increasing trend of NAD(P)H signal (n=14 images).

Supplementary Figure 3

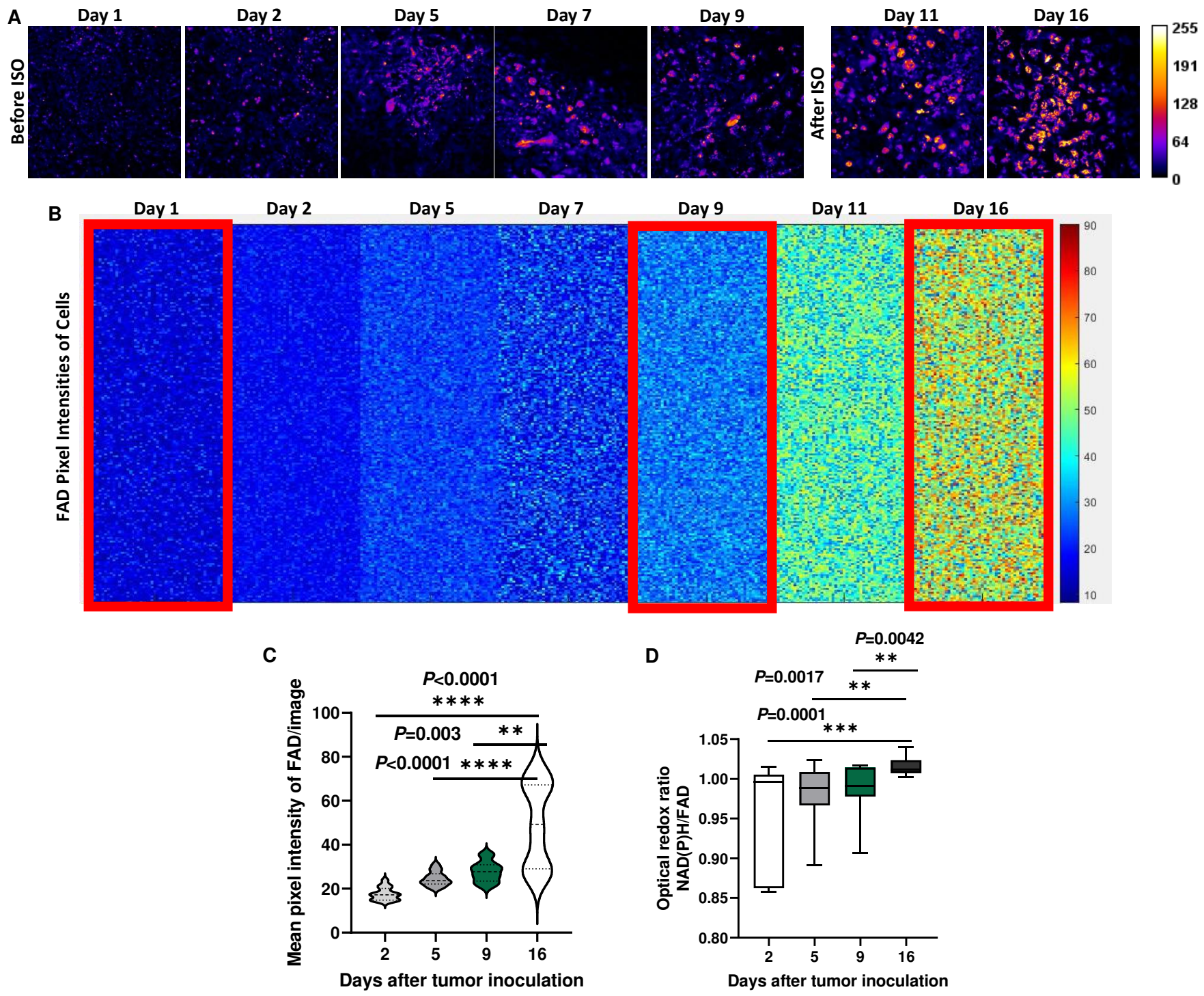

Dynamic metabolic imaging of FAD before and after treatment of isotype control antibody. **(A)** Label-free metabolic intravital imaging (LMMI) of FAD before and after treatment of isotype control antibody showing continuous tumor growth (10 mg/kg intravenous injection daily for 5 days). **(B)** Kinetics of single cell metabolism with FAD signal. Each colored small square represents the visible pixel intensity of FAD in each cancer cell. 10,000-pixel intensities were randomly measured from the cells in different mice every day for 16 days (n=5 mice). Metabolic signal of NAD(P)H has been increased with tumor growth from Day 1 to Day 9 and continued to increase even with start of isotype control treatment from Day 10 as expected. **(C)** Quantification of average intensity shows clear increasing trend of FAD signal (n=14 images). **(D)** Optical redox ratio measurement shows a similar increasing trend (n=14 images).

Supplementary Figure 4

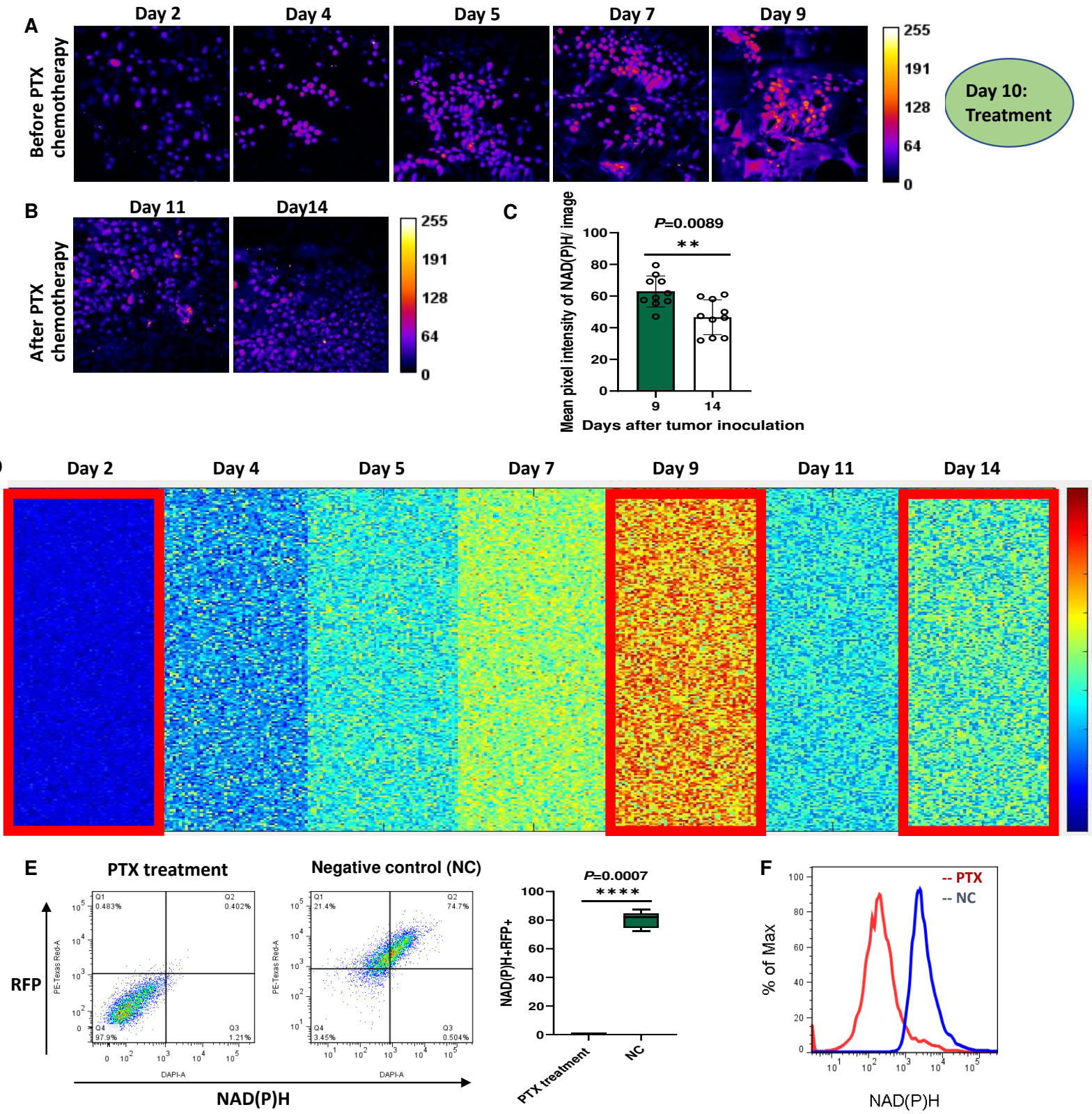

Sensitive monitoring of paclitaxel chemotherapy response by dynamic metabolic imaging of NAD(P)H. (A, B) Label-free metabolic intravital imaging (LMII) of NAD(P)H demonstrates sensitive early response at single-cell level after paclitaxel (PTX) treatment (10 mg/kg intraperitoneal injection on Day 10). **(C)** Quantification of average intensity shows statistically significant difference in NAD(P)H signals before and after PTX treatment (n=10 images, *P*=0.0089 for Day 9 and Day 14). **(D)** Kinetics of single cell metabolism with NAD(P)H signal. Each colored small square represents the visible pixel intensity of NAD(P)H in each cancer cell. 10,000-pixel intensities were randomly measured from the cells in different mice every day for 16 days (n=8 mice). Metabolic signal of NAD(P)H has been increased with tumor growth from Day 1 to Day 9 and dramatically decreased with start of PTX treatment from Day 10. **(E)** Flow cytometric analysis shows decrease of NAD(P)H+RFP+ cells after PTX treatment (n=15 mice, *P*=0.0007). **(F)** Decreased NAD(P)H signal with PTX treatment compared to negative control treatment was confirmed by flow cytometry.

Supplementary Figure 5

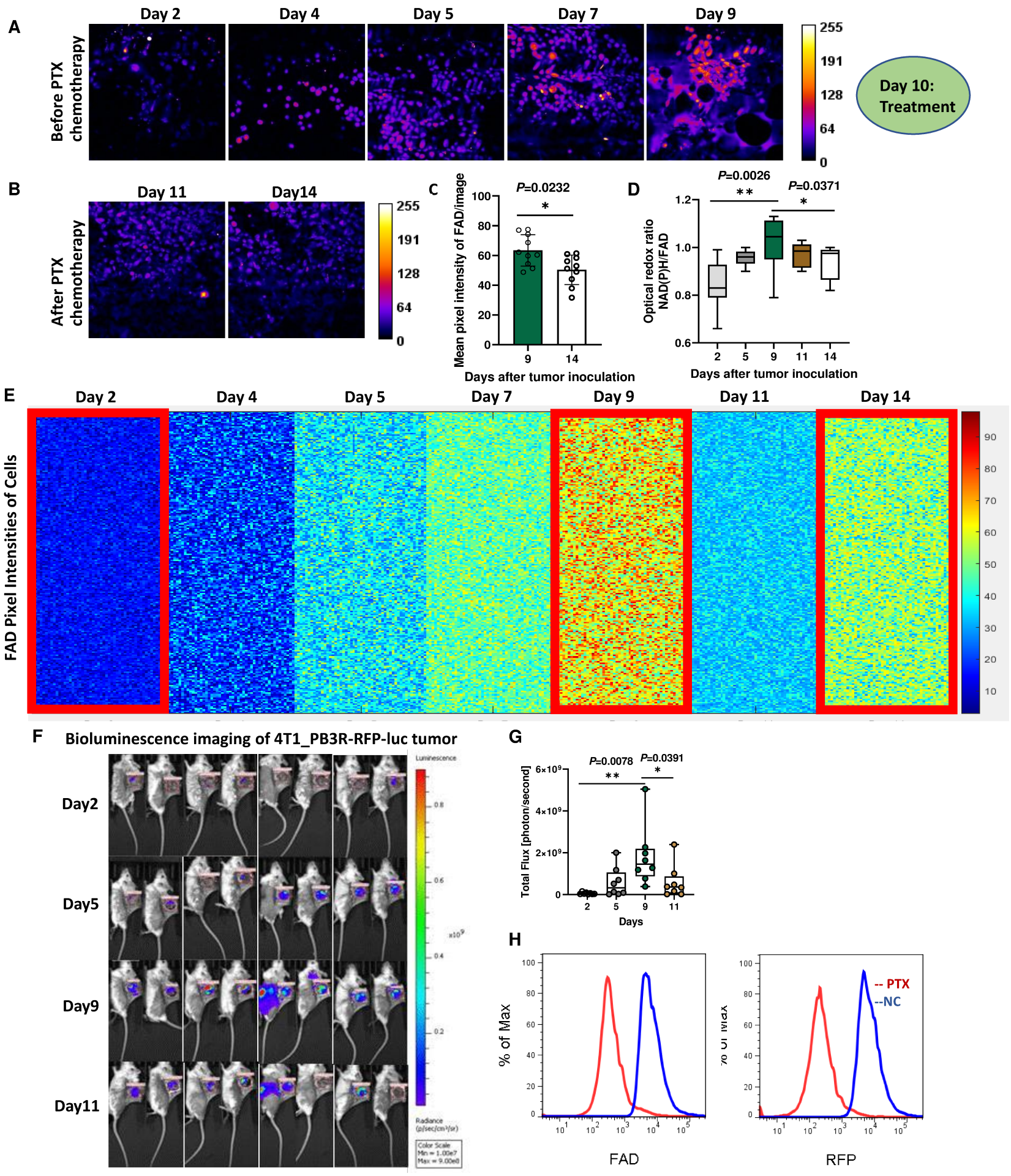

Sensitive monitoring of paclitaxel chemotherapy response by dynamic metabolic imaging of FAD. (A, B) Label-free metabolic intravital imaging (LMII) of FAD demonstrates sensitive early response at single-cell level after paclitaxel (PTX) treatment (10 mg/kg intraperitoneal injection daily for 5 days). **(C)** Quantification of average intensity shows statistically significant difference in FAD signals before and after PTX treatment (n=10 images, *P*=0.0232). **(D)** Optical redox ratio was increased with tumor growth and decreased with PTX treatment (n=10 images, *P*=0.0371 for Day 9 and Day 14). **(E)** Kinetics of single cell metabolism with FAD signal. Each colored small square represents the visible pixel intensity of FAD in each cancer cell. 10,000-pixel intensities were randomly measured from the cells in different mice every day for 16 days (n=8 mice). Metabolic signal of FAD has been increased with tumor growth from Day 1 to Day 9 and dramatically decreased with start of PTX treatment from Day 10. **(F, G)** Conventional whole-body bioluminescence imaging of 4T1_PB3R-RFP-luc tumor mice verified cancer treatment with increased signal before PTX therapy and decreased signal after PTX therapy. LMMI shows better sensitivity to detect chemotherapy response (*P*=0.0232 in **C**) over bioluminescence imaging (*P*=0.0391 in **G**). **(H)** Flow cytometric analysis shows decrease of FAD+ cells and 4T1_PB3R-RFP+ cells after PTX treatment.

Supplementary Figure 6

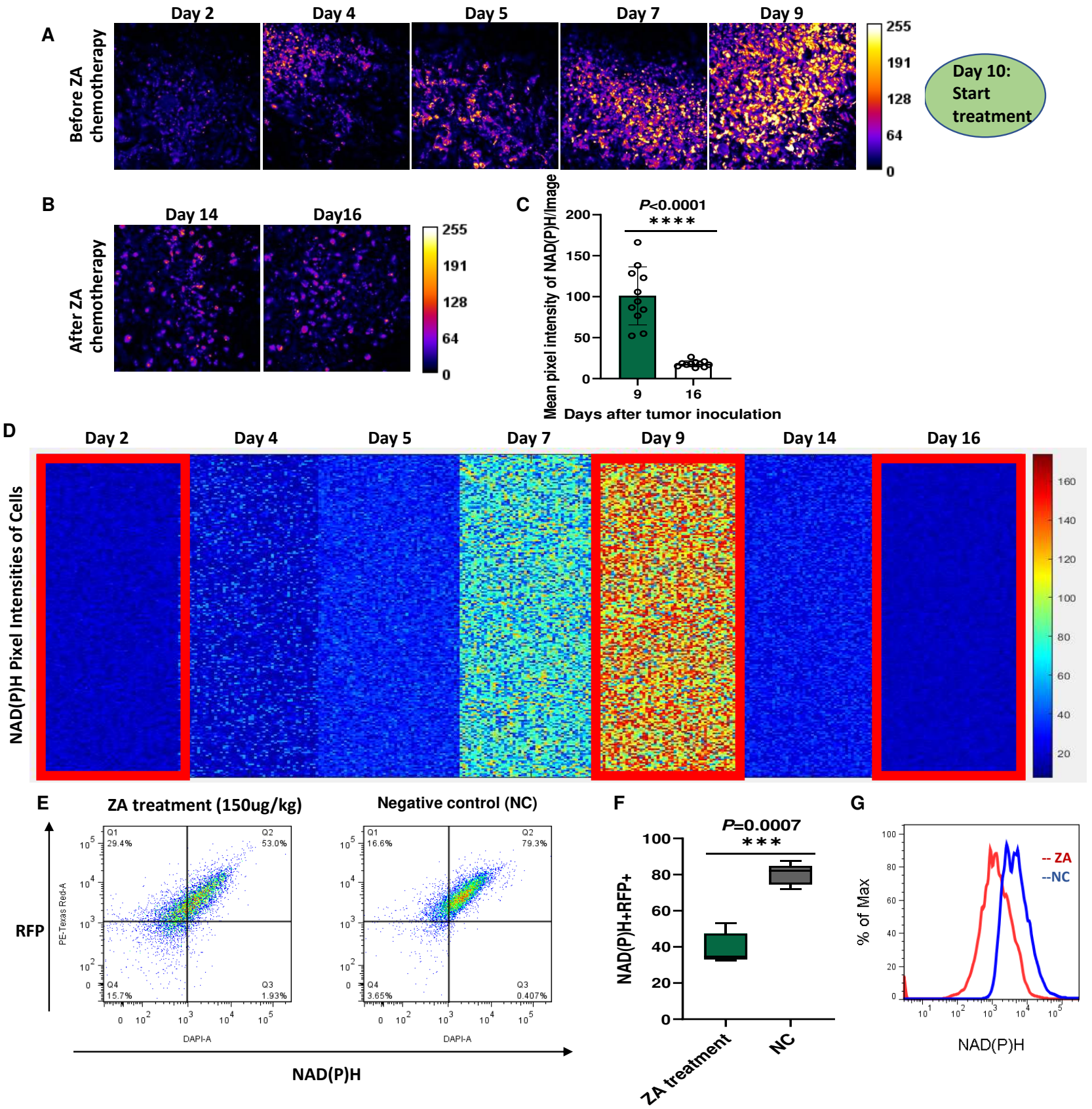

Sensitive monitoring of zoledronic acid chemotherapy response by dynamic metabolic imaging of NAD(P)H. (A, B) Label-free metabolic intravital imaging (LMII) of NAD(P)H demonstrates sensitive early response at single-cell level after zoledronic acid (ZA) treatment (150 µg/kg intraperitoneal injection daily for 5 days). **(C)** Quantification of average intensity shows statistically significant difference in NAD(P)H signals before and after ZA treatment (n=11 images, *P*<0.0001 for Day 9 and Day 16). **(D)** Kinetics of single cell metabolism with NAD(P)H signal. Each colored small square represents the visible pixel intensity of NAD(P)H in each cancer cell. 10,000-pixel intensities were randomly measured from the cells in different mice every day for 16 days (n=6 mice). Metabolic signal of NAD(P)H has been increased with tumor growth from Day 1 to Day 9 and dramatically decreased with start of ZA treatment from Day 10. **(E)** Flow cytometric analysis shows decrease of NAD(P)H+RFP+ cells after ZA treatment (n=15 mice, *P*=0.0007). **(E)** Decreased NAD(P)H signal with ZA treatment compared to negative control treatment was confirmed by flow cytometry.

Supplementary Figure 7

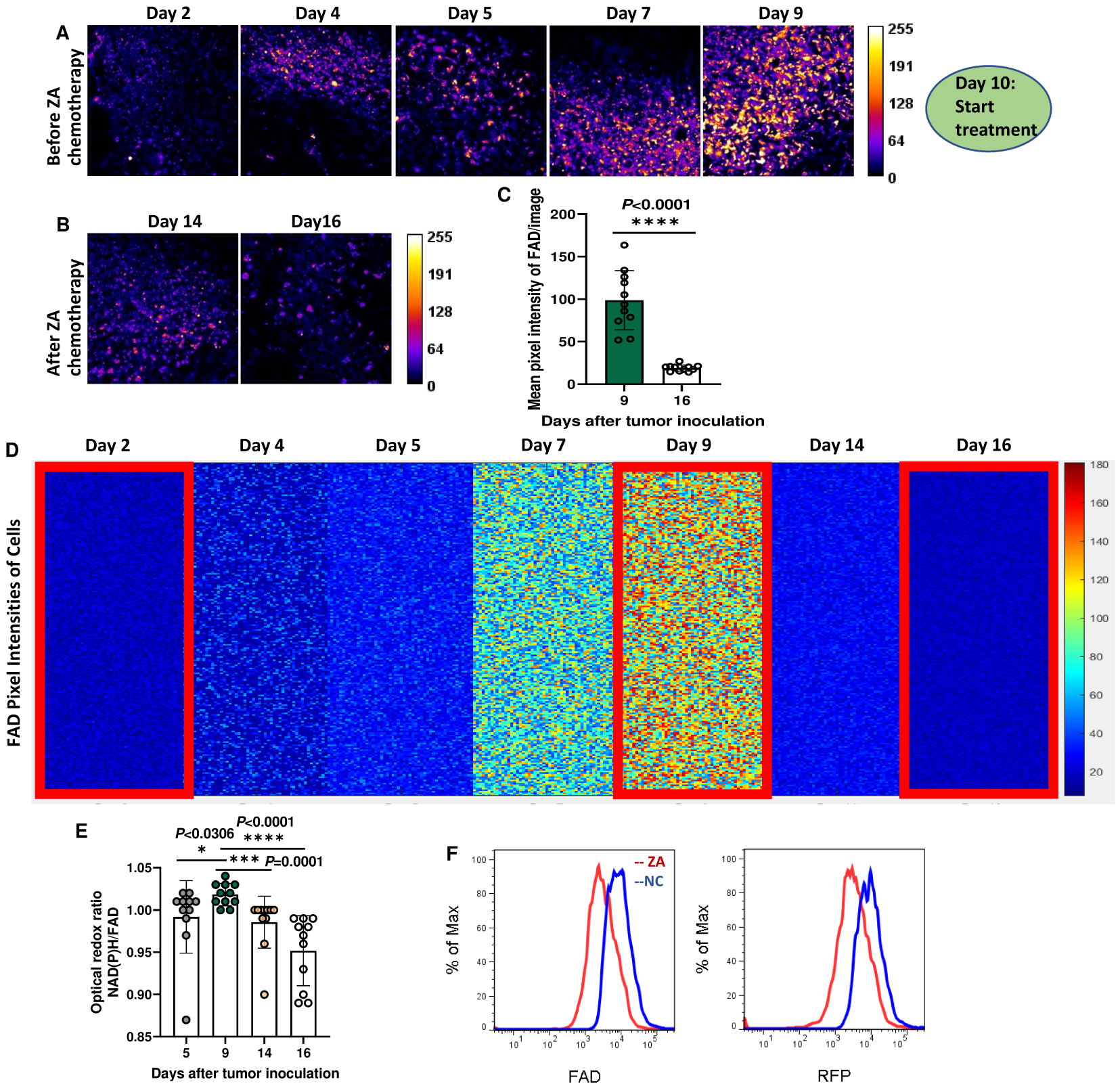

Sensitive monitoring of zoledronic acid chemotherapy response by dynamic metabolic imaging of FAD. (A, B) Label-free metabolic intravital imaging (LMII) of FAD demonstrates sensitive early response at single-cell level after zoledronic acid (ZA) treatment (150 µg/kg intraperitoneal injection daily for 5 days). **(C)** Quantification of average intensity shows statistically significant difference in FAD signals before and after ZA treatment (n=11 images, $P<0.0001$ for Day 9 and Day 16). **(D)** Kinetics of single cell metabolism with FAD signal. Each colored small square represents the visible pixel intensity of FAD in each cancer cell. 10,000-pixel intensities were randomly measured from the cells in different mice every day for 16 days (n=6 mice). Metabolic signal of FAD has been increased with tumor growth from Day 1 to Day 9 and dramatically decreased with start of ZA treatment from Day 10. **(E)** Optical redox ratio was increased with tumor growth and decreased with ZA treatment (n=15 mice, $P<0.0001$ for Day 9 and Day 14). **(F)** Flow cytometric analysis shows decrease of FAD+ cells and 4T1_PB3R-RFP+ cells after ZA treatment.

Supplementary Figure 8

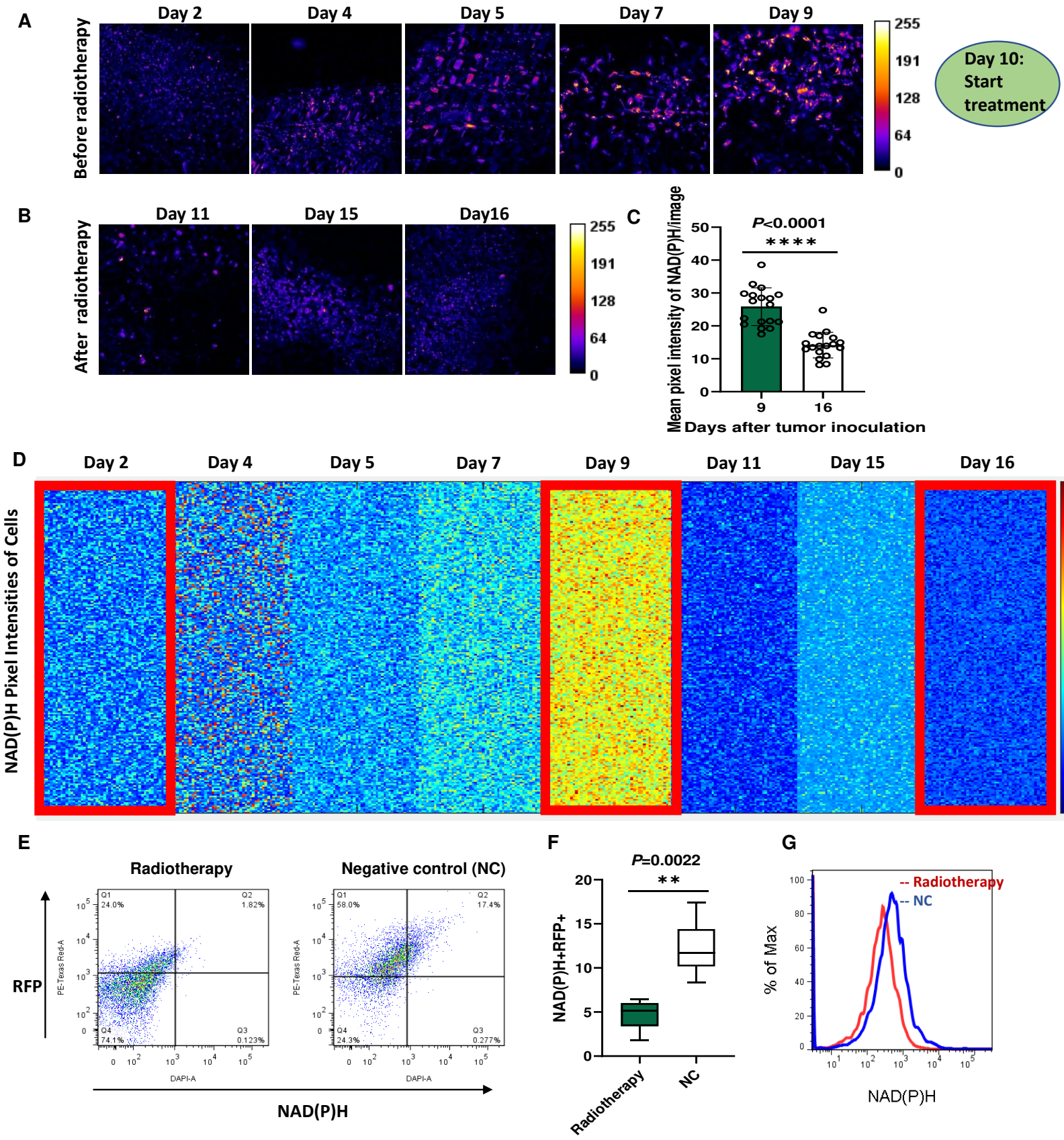

Sensitive monitoring of radiotherapy response by dynamic metabolic imaging of NAD(P)H. (A, B) Label-free metabolic intravital imaging (LMII) of NAD(P)H demonstrates sensitive early response at single-cell level after radiotherapy (2 Gy/daily for 4 days, rate 1.8 Gy/min). **(C)** Quantification of average intensity shows statistically significant difference in NAD(P)H signals before and after radiation treatment (n=18 images, *P*<0.0001 for Day 9 and Day 16). **(D)** Kinetics of single cell metabolism with NAD(P)H signal. Each colored small square represents the visible pixel intensity of NAD(P)H in each cancer cell. 10,000-pixel intensities were randomly measured from the cells in different mice every day for 16 days (n=6 mice). Metabolic signal of NAD(P)H has been increased with tumor growth from Day 1 to Day 9 and dramatically decreased with start of radiation treatment from Day 10. **(E, F)** Flow cytometric analysis shows decrease of NAD(P)H+RFP+ cells with radiation treatment compared to negative control (n=12 mice, *P*=0.0022). **(G)** Decreased NAD(P)H signal with radiation treatment compared to negative control was confirmed by flow cytometry.

Supplementary Figure 9

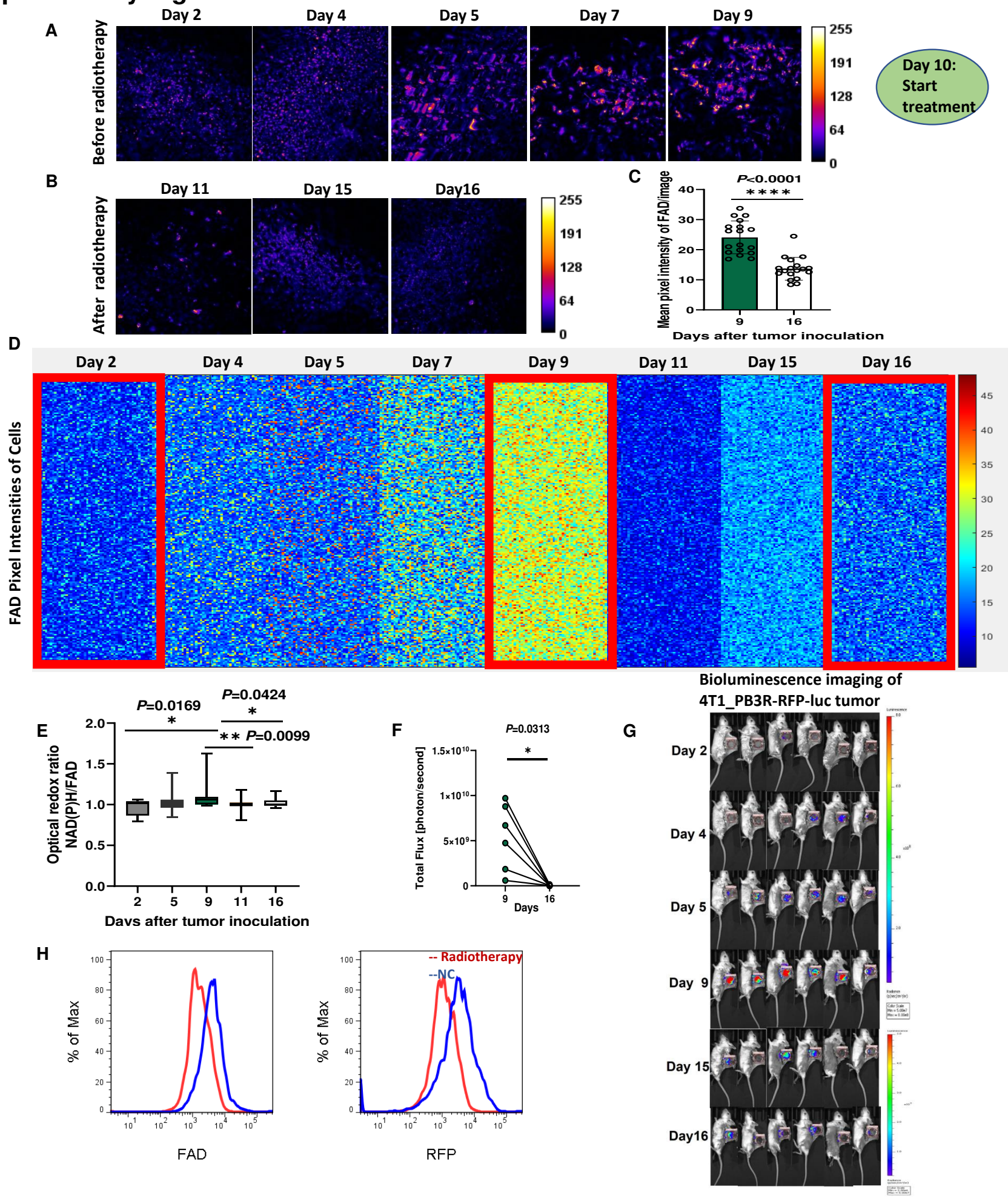

Sensitive monitoring of radiotherapy response by dynamic metabolic imaging of FAD. (A, B) Label-free metabolic intravital imaging (LMII) of FAD demonstrates sensitive early response at single-cell level after radiation treatment (2 Gy/daily for 4 days, rate 1.8 Gy/min). **(C)** Quantification of average intensity shows statistically significant difference in FAD signals before and after radiation treatment (n=18 images, $P<0.0001$). **(D)** Kinetics of single cell metabolism with FAD signal. Each colored small square represents the visible pixel intensity of FAD in each cancer cell. 10,000-pixel intensities were randomly measured from the cells in different mice every day for 16 days (n=6 mice). Metabolic signal of FAD has been increased with tumor growth from Day 1 to Day 9 and dramatically decreased with start of radiation treatment from Day 10. **(E)** Optical redox ratio was increased with tumor growth and decreased with radiation treatment (n=6, $P=0.0424$ for Day 9 and Day 14). **(F, G)** Conventional whole-body bioluminescence imaging of 4T1_PB3R-RFP-luc tumor mice verified cancer treatment with increased signal before radiotherapy and decreased signal after radiotherapy (n=6 mice). LMMI shows better sensitivity to detect radiotherapy response ($P<0.0001$ in **C**) over bioluminescence imaging ($P=0.0313$ in **F**). **(H)** Flow cytometric analysis shows decrease of FAD+ cells and 4T1_PB3R-RFP+ cells after radiation treatment.

Supplementary Figure 10

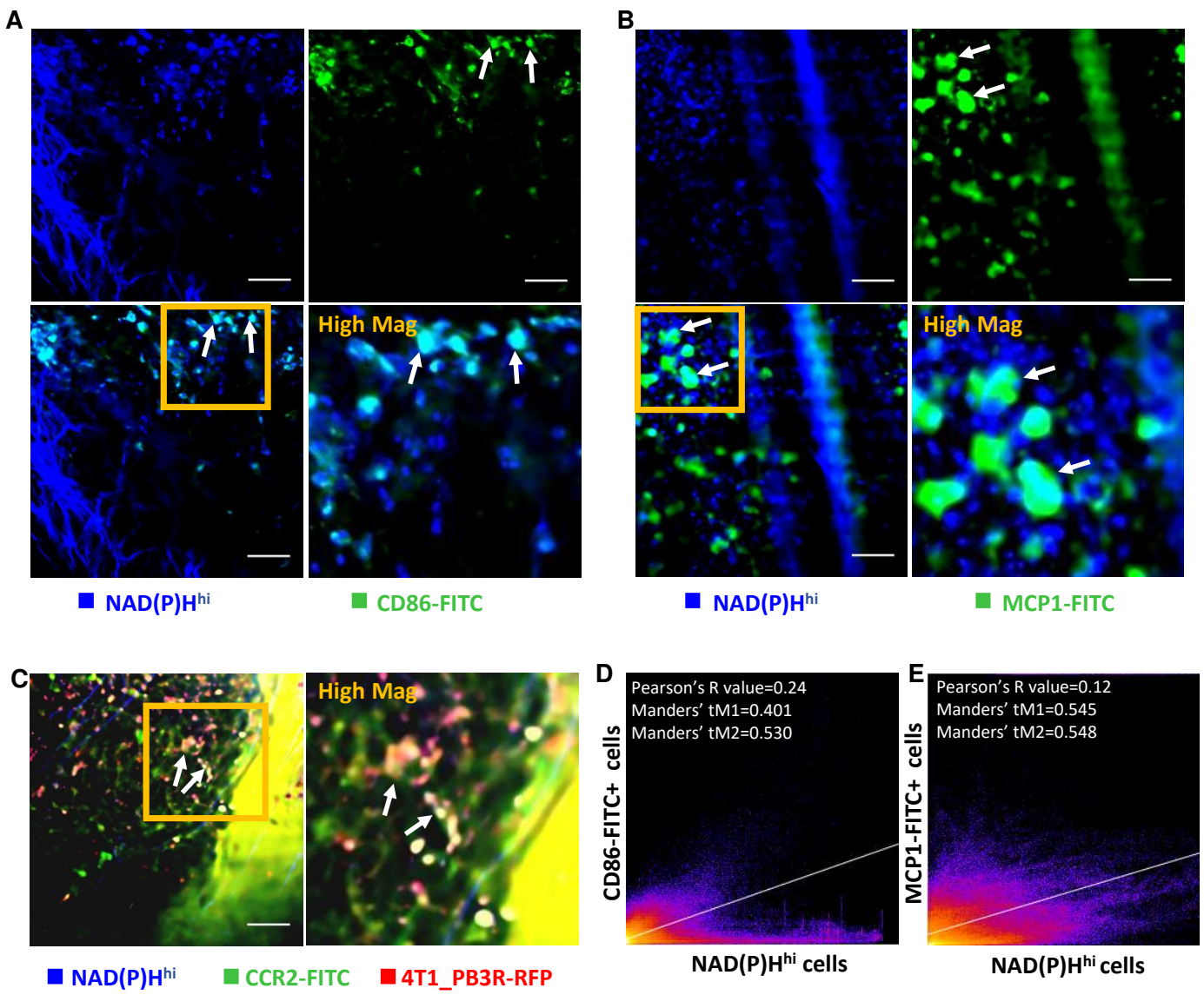

Intravital imaging reveals co-localization of NAD(P)H^{hi} cells and M1 macrophages in tumor microenvironment. (A) Representative intravital images of NAD(P)H^{hi} cells (blue) and CD86-FITC+ cells (green). Arrows indicate *in vivo* co-localization of NAD(P)H^{hi} cells and CD86-FITC+ cells. **(B)** Representative intravital images of NAD(P)H^{hi} cells (blue) and MCP1-FITC+ cells (green). Arrows indicate in vivo co-localization of NAD(P)H^{hi} cells and MCP1-FITC+ cells. **(C)** Representative intravital images of NAD(P)H^{hi} cells (blue), 4T1_PB3R-RFP+ cells (red), and CCR2-FITC+ cells (green). Arrows indicate *in vivo* co-localization of NAD(P)H^{hi} cells and CCR2-FITC+ cells. Scales, 20 µm. **(D)** Quantitative co-localization analysis using Pearson's coefficient and Manders coefficients revealed that a small portion of NAD(P)H^{hi} cells are targeting immune-active M1 macrophages visualized by fluorescent CD86 antibody or specific peptide based fluorescent probes targeting MCP1 or CCR2 in triple-negative breast cancer models. Scales, 20 µm.

Supplementary Figure 11

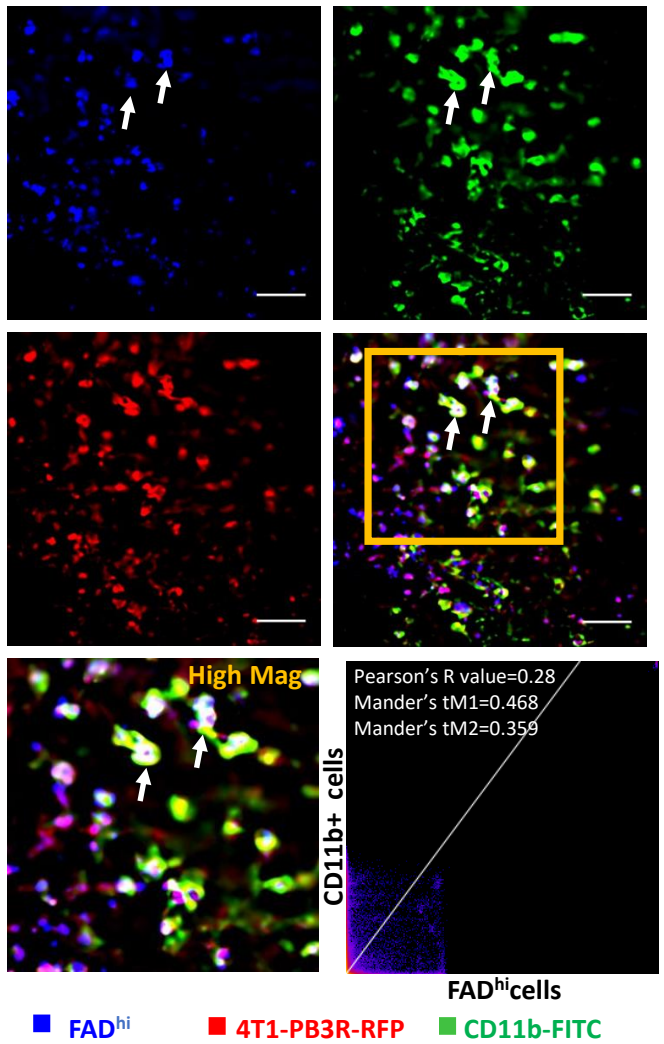

Intravital imaging reveals co-localization of FAD^{hi} and CD11b+ macrophages in tumor microenvironment. Representative intravital images of FAD^{hi} cells (blue), 4T1_3BR-RFP+ cells (red), and CD11b+ macrophages (green) in a mouse model of triple-negative breast cancer. Arrows indicate *in vivo* co-localization of FAD^{hi} cells and CD11b+ macrophages. Quantitative co-localization analysis using Pearson's coefficient and Manders coefficients revealed targeting ability of metabolic FAD imaging for CD11b+ macrophages. Scales, 20 μm.

Supplementary Figure 12

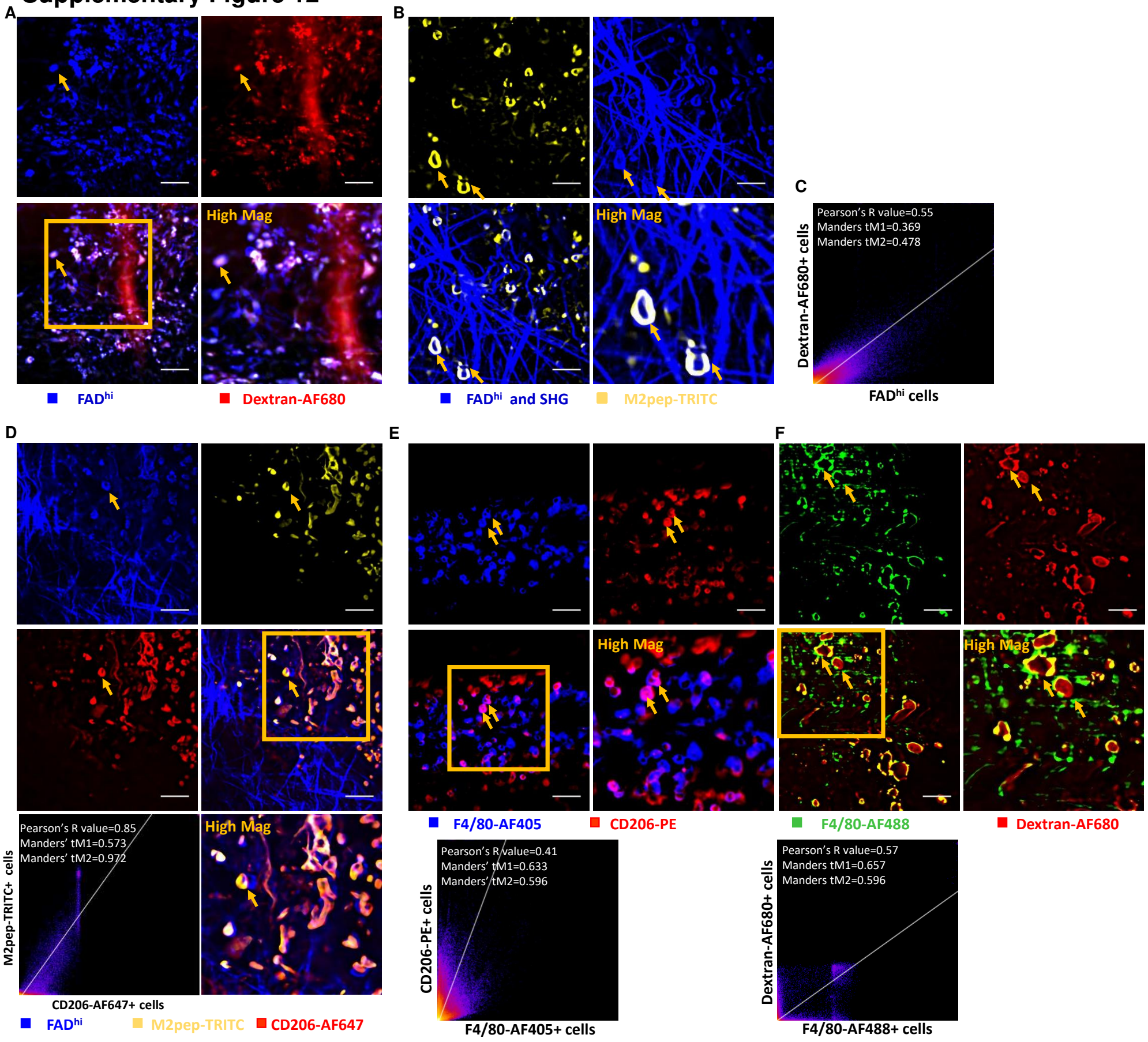

Intravital imaging reveals co-localization of FAD^{hi} cells and M2 macrophages in tumor microenvironment. (A) Representative intravital images of FAD^{hi} cells (blue) and Dextran-AF680+ cells (red). **(B)** Representative intravital images of FAD^{hi} cells (green) and M2pep-TRITC+ cells (yellow). **(C)** A scatter plot depicting quantitative co-localization analysis between FAD^{hi} cells and Dextran-AF680+ cells using Pearson's coefficient and Manders coefficients. **(D)** Representative intravital images of FAD^{hi} cells (blue), M2pep-TRITC+ cells (yellow), and CD206-AF607+ cells (red) and a scatter plot showing quantitative co-localization analysis. **(E)** Representative intravital images of F4/80-AF405+ cells (blue) and CD206-PE+ cells (yellow) and a scatter plot showing quantitative co-localization analysis. **(F)** Representative intravital images of F4/80-AF488+ cells and Dextran-AF680+ cells and a scatter plot showing quantitative co-localization analysis. *In vivo* co-localization analysis shows specific targeting ability of metabolic FAD imaging for immunosuppressive M2 macrophages visualized by high uptake of Dextran-AF680 or by M2 macrophage specific peptide based fluorescent imaging probe, M2pep-TRITC in triple-negative breast cancer models. *In vivo* targeting ability of M2pep-TRITC and Dextran-AF680 was verified by *in vivo* immunostaining using CD206 or F4/80. Scales, 20 µm. Representative co-localized cells are indicated by arrows.

Supplementary Figure 13

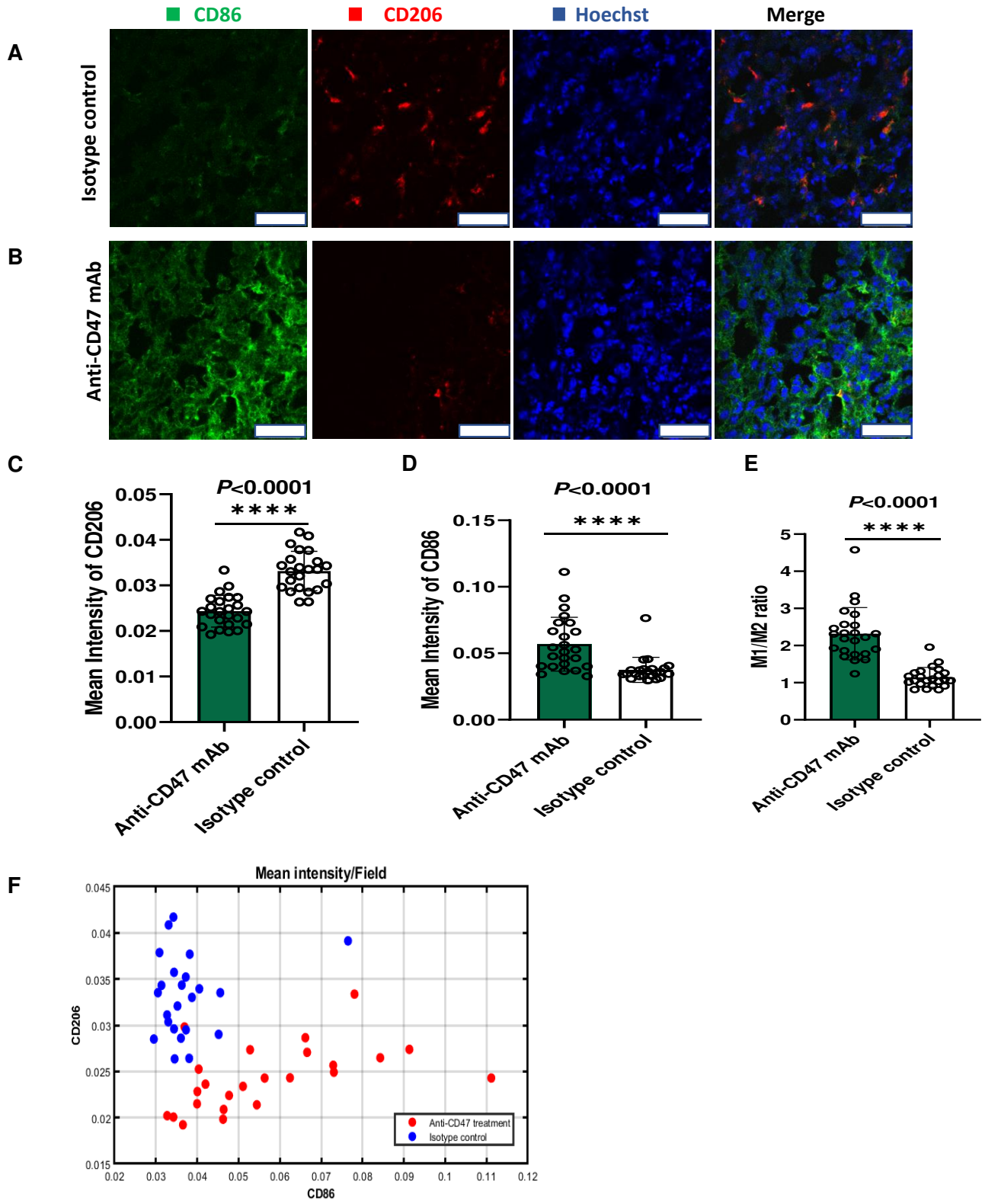

Histological examination of tumor-associated macrophages' polarization by anti-CD47 therapy. (A, B) Representative immunofluorescence images stained by anti-CD86 and anti-CD206 antibodies in 4T1 tumor tissue 5 days post injection of isotype control antibody or anti-CD47 mAb in mouse models of triple-negative breast cancer. Scales, 25 µm. **(C, D)** Quantitative average intensity analysis showing that anti-CD47 mAb treatment inhibited CD206+ immunosuppressive M2 macrophages and promoted CD86+ immune-active phagocytotic M1 macrophages (P<0.0001 between anti-CD47 mAb and isotype control antibody treated tumors) **(E, F)** A high M1/M2 ratio is detected in 4T1 tumor-bearing mice with anti-CD47 mAb treatment for 5 days (P<0.0001 between anti-CD47 mAb and isotype control antibody treated tumors).

Supplementary Figure 14

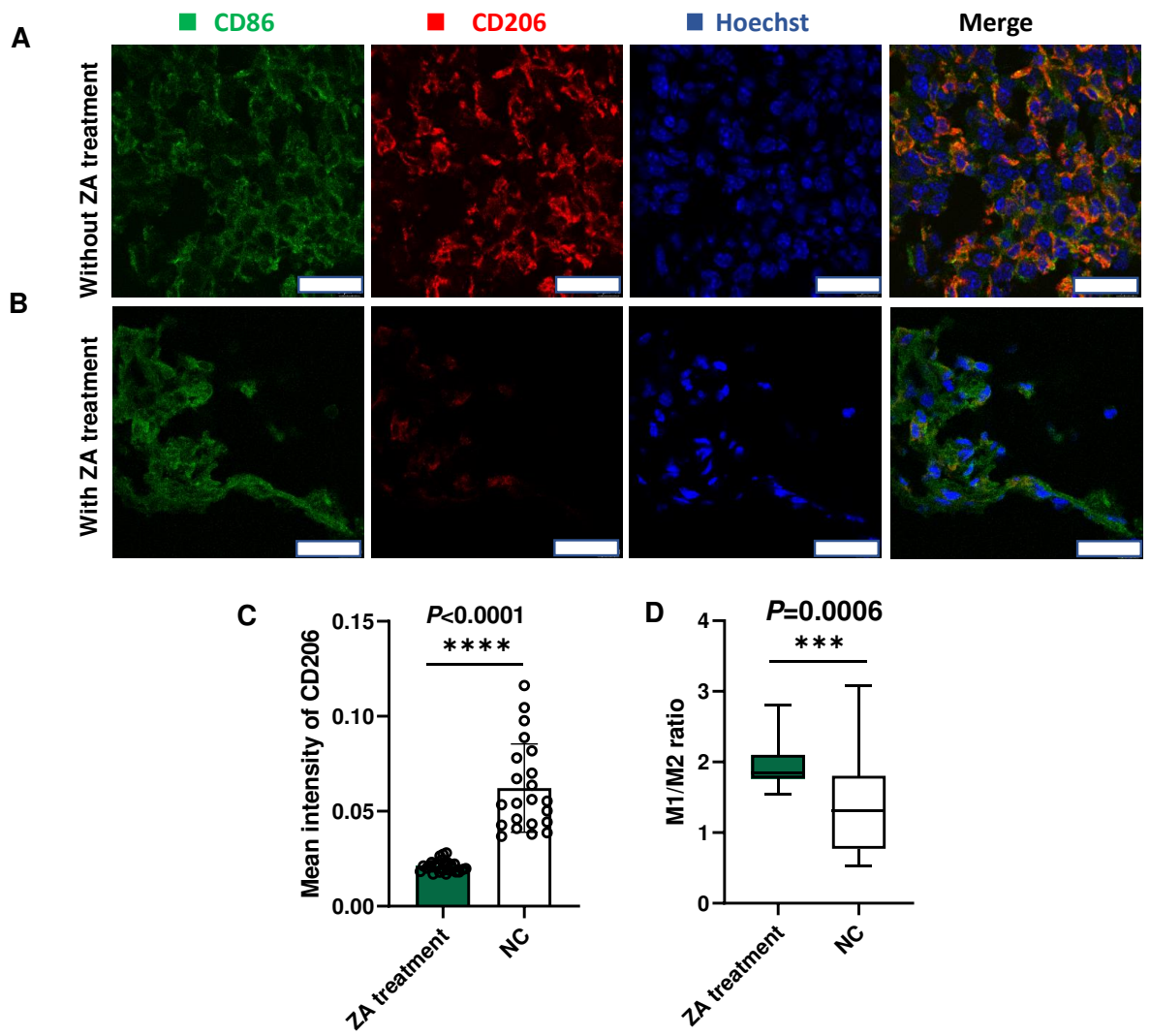

Histological examination of tumor-associated macrophages' polarization by zoledronic acid chemotherapy. (A, B) Representative immunofluorescence images stained by anti-CD86 and anti-CD206 antibodies in 4T1 tumor tissue 5 days post injection of negative control or zoledronic acid chemotherapy in mouse models of triple-negative breast cancer. Scales, 25 μm. **(C)** Quantitative average intensity analysis showing that zoledronic acid chemotherapy inhibited CD206+ immunosuppressive M2 macrophages (P<0.0001 between zoledronic acid chemotherapy and negative control treated tumors) **(D)** A high M1/M2 ratio is detected in 4T1 tumor-bearing mice with zoledronic acid chemotherapy for 5 days (P=0.0006 between zoledronic acid chemotherapy and negative control treated tumors).

Supplementary Figure 15

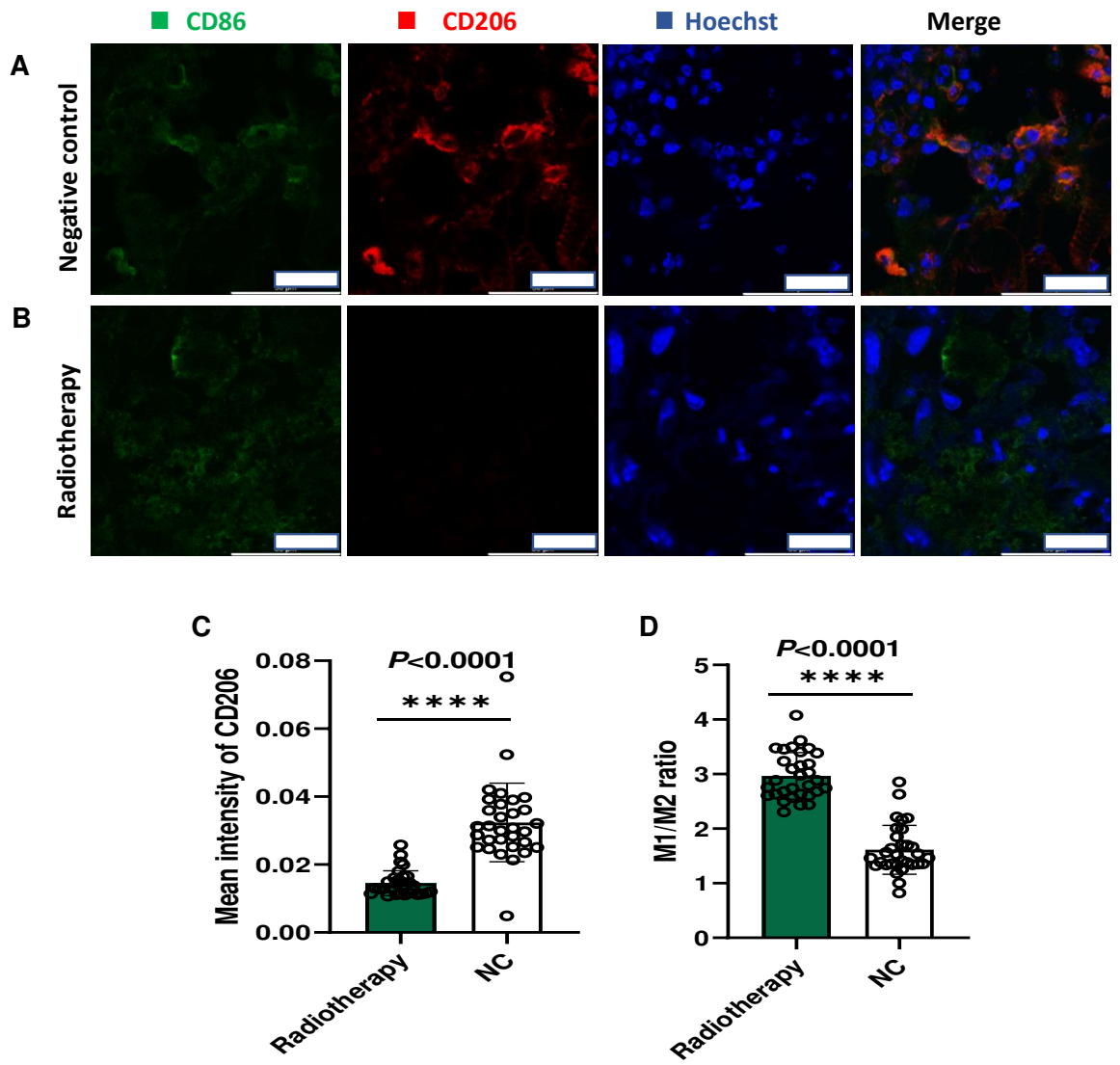

Histological examination of tumor-associated macrophages' polarization by radiotherapy. (A, B) Representative immunofluorescence images stained by anti-CD86 and anti-CD206 antibodies in 4T1 tumor tissue after radiotherapy (2 Gy/daily for 4 days, rate 1.8 Gy/min) in mouse models of triple-negative breast cancer. Scales, 25 μm. **(C)** Quantitative average intensity analysis showing that radiation treatment inhibited CD206+ immunosuppressive M2 macrophages (P<0.0001 between radiotherapy and negative control treated tumors) **(D)** A high M1/M2 ratio is detected in 4T1 tumor-bearing mice with radiation treatment for 4 days (P<0.0001 between radiotherapy and negative control treated tumors).

Supplementary Table 1

Lists of antibodies, imaging probes, immune checkpoint inhibitors, and chemotherapeutic drugs

Immune-active cells	NAD(P)H^{hi} cells	Antibodies or imaging probes
Helper T cells	Colocalization	CD4-FITC mAb (BD Biosciences, USA, 1:3 dilution)
Dendritic cells	Colocalization	CD11c-FITC mAb (BD Biosciences, USA, 1:3 dilution)
Pan macrophages	Colocalization	F4/80-PE mAb, F4/80-AF488 mAb (Abcam, 1:3 dilution)
M1 macrophages	Colocalization	MCP1-FITC (150 µg/mouse diluted in 100 µl of 1% BSA-PBS); CD86-FITC mAb (BD Biosciences, USA, 1:3 dilution)
M1 macrophages	Colocalization	CCR2-FITC (30 µg/mouse diluted in 100 µl of 1% BSA-PBS)

Immunosuppressive cells	FAD^{hi} cells	Antibodies or imaging probes
M2 macrophages	Colocalization	CD206-AF647 mAb (BD Biosciences, USA, 1:3 dilution)
M2 macrophages	Colocalization	CD301b-AF647 mAb (Biolegend, USA, 1:3 dilution)
M2 macrophages	Colocalization	CD11b-FITC mAb (BD Biosciences, USA, 1:3 dilution)
M2 macrophages	Colocalization	M2pep-TRITC (150 µg/mouse diluted in 100 µl of 1% BSA-PBS)
M2 macrophages	Colocalization	Dextran-AF680 (450 µg/mouse diluted in 100 µl of 1% BSA-PBS)
Regulatory T cells	Colocalization	CD4-FITC mAb (BD Biosciences, USA, 1:3 dilution) and CD25-PE mAb (BD Biosciences, USA, 1:3 dilution)

CD47-SIRPα pathway	Antibodies
CD47 antigens	anti-mouse CD47-AF488 mAb
Pan macrophages	F4/80-PE mAb (Abcam, USA)

Comparative studies	Reagents or imaging probes
Whole-body bioluminescence imaging by IVIS	D-luciferins (Promega, USA)
Whole-body fluorescent glucose imaging by IVIS	IVISense 2-DG 750 Fluorescent Probe in RediJect™ Solution (PerkinElmer, USA)

Treatments	Antibodies and drugs
Immunotherapy (MIAP301)	anti-mouse CD47 mAb (clone MIAP301, Rat IgG2a, κ, BioXcell, USA)
Immunotherapy (Isotype control)	Rat IgG2a isotype control mAb (clone 2A3, Rat IgG2a, κ, BioXcell, USA)
Chemotherapy	Paclitaxel (PTX) (SelleckChem, USA)
Chemotherapy	Zoledronic acid (ZA) (SelleckChem, USA)

Supplementary Video Legends

Supplementary Video 1

Skinfold window chamber models with transplantation of 4T1-PB3R-RFP+ murine triple-negative breast cancer cells

Supplementary Video 2

***In vivo* observation of co-localization among NAD(P)H^{hi} metabolic signal, F4/80+ macrophages, and anti-CD47 mAb treated cancer cells.** A large number of co-localized cells among different populations of NAD(P)H^{hi} cell (blue), F4/80-PE targeted macrophages (red), and CD47-AF488 targeted cancer cells (green) are observed by intravital imaging. Using a window chamber model of 4T1 triple-negative breast cancer, label-free metabolic intravital imaging of NAD(P)H enabled visualization of anti-CD47 drug (green) accumulation in NAD(P)H^{hi} cancer cells (blue) and engulfment of cancer cells by F4/80+ macrophages (red) following subcutaneous injection of a mixture of anti-F4/80-PE mAb and anti-CD47-AF488 mAb in 1% BSA-PBS under fascia.

Supplementary Video 3

***In vivo* observation of antibody-dependent cellular phagocytosis (ADCP) events.** Upon the administration of anti-CD47-AF488 mAb and anti-F4/80-PE mAb, ADCP events were observed as rapid but short waves between F4/80-PE labeled macrophages (red) and CD47-AF488 mAb treated cancer cells (green). Fibrillary structures (blue) indicate collagen visualized by second harmonic generation.

Supplementary Video 4

***In vivo* observation of antibody-dependent cellular phagocytosis (ADCP) events using NAD(P)H metabolic imaging.** Upon the administration of anti-CD47-AF488 mAb and anti-F4/80-PE mAb, ADCP events were observed as rapid but short waves between F4/80-PE labeled macrophages (red) and NAD(P)H^{hi} cancer cells (blue) in a skinfold mouse cancer model.

Supplementary Video 5

Representative intravital imaging showing high overlap between NAD(P)H^{hi} cells and CD11c+ dendritic cells. *In vivo* immunofluorescence staining by subcutaneous injection anti-CD11c-FITC mAb demonstrated high co-localization between NAD(P)^{hi} cells (blue) and immune-active CD11c+ dendritic cells in a skinfold mouse cancer model. 4T1_PB3R-RFP+ cancer cells (red) were imaged together.

Supplementary Video 6

Representative intravital imaging showing high overlap between NAD(P)H^{hi} cells and MCP1-FITC labelled M1 macrophages. Tail vein administration of MCP1-FITC imaging probe in a skinfold mouse cancer model enables evaluation of *in vivo* targeting ability of metabolic NAD(P)H imaging toward immune-active phagocytotic M1 macrophages. MCP1-FITC labelled macrophages are shown in green, 4T1-PB3R-RFP+ cancer cells are shown in red, and NAD(P)H^{hi} cells are shown in blue.

Supplementary Video 7

Representative intravital imaging showing high overlap between NAD(P)H^{hi} cells and CCR2-FITC labelled M1 macrophages. Tail vein administration of CCR2-FITC imaging probe in a skinfold mouse cancer model enables evaluation of *in vivo* targeting ability of metabolic NAD(P)H imaging toward immune-active phagocytotic M1 macrophages. CCR2-FITC labelled macrophages are shown in green, 4T1-PB3R-RFP+ cancer cells are shown in red, and NAD(P)H^{hi} cells are shown in blue.